Using Airborne Hydromapping to Study an Alpine Torrent

W. Dobler, R. Baran, F. Steinbacher, M. Ritter
AirborneHydroMapping GmbH, Innsbruck, Austria
M. Aufleger
University of Innsbruck, Unit of Hydraulic Engineering, Department of Infrastructure, Innsbruck, Austria

ABSTRACT: Knowledge about the hydraulics in alpine torrents is relevant to quantify flood risks, to study sediment transport and to assess the water-bodies ecology. Usually, computational fluid dynamics (CFD) simulations are the preferred tool to calculate velocities, water depths and sediment transport for the discharges of interest, which then serve as a basis for the evaluation of flood risks or ecological conditions. To enable reliable calculations, high-quality terrain data of the riverbeds, riverbanks, and floodplains are required. Typically, DTMs of the floodplains reconstructed from airborne light detection and ranging (LiDAR) data are combined with terrestrial surveys of riverbanks and riverbeds. The terrestrial surveys are necessary as the lasers usually cannot penetrate the water surface in the observed water-bodies. They are labor intensive and can be located in difficultly accessible terrain. Therefore, data of the riverbeds' and riverbanks' geometry is hardly available at such a high resolution and extent that is comparable to the airborne LiDAR based data of the floodplains. In this study a newly available airborne water-penetrating LiDAR system was used to survey alpine torrents. Detailed and extensive data of riverbeds and riverbanks were acquired. The general applicability of the data as a basis for a Telemac-2D simulation was investigated. Mesh creation based on breaking edges or on a downsampled point cloud are shown. Finally, a calibration was done based on abundant water surface points stemming from the airborne-laser scanning. The LiDAR data turned out to be a very suitable data source for constructing the computational grids of the riverbed. The CFD results showed new possibilities in the comparison of measured and simulated water heights.

1 INTRODUCTION

For water engineering one of the most important aspects of hydraulics deals with representing the topography of rivers, floodplains, estuaries or coastal areas. The hydraulic background of water bodies in terms of 2D- or 3D-modeling is influenced by various factors. Among these factors, differences exist in scale and resolution but those differences need to be considered to derive close-to-reality numerical models. Commonly, flood or wave model applications utilize digital elevation models based on high-quality and high-resolution topographic airborne laser data (Fig. 1). The digital elevation model of a water body itself is normally represented by simplified and interpolated data based on cross-sections, manually collected during terrestrial fieldwork or by echosounder data. Due to a lack of spatial and high-resolution water-body information, the modelling of shallow areas like meadows, estuaries, riverbanks or dune structures is highly time consuming, or even impossible (Fig. 1). Frequent urban or coastal flooding over the past decades have identified an urgent need to improve and increase our modelling efforts, and to address more explicitly the focus on effects of uncertainty in simulations caused by model input data. Society demands reliable and detailed information on magnitude and likelihood of hazardous flood events to design flood mitigation. For this, the assumption of the shape of the water body or manmade protection structures has to be solved and modelling improved by using the actual shape. Furthermore, additional information like surface roughness or the water surface are relevant to calibrate such models. The technology of hydromapping aims to solve this challenge.

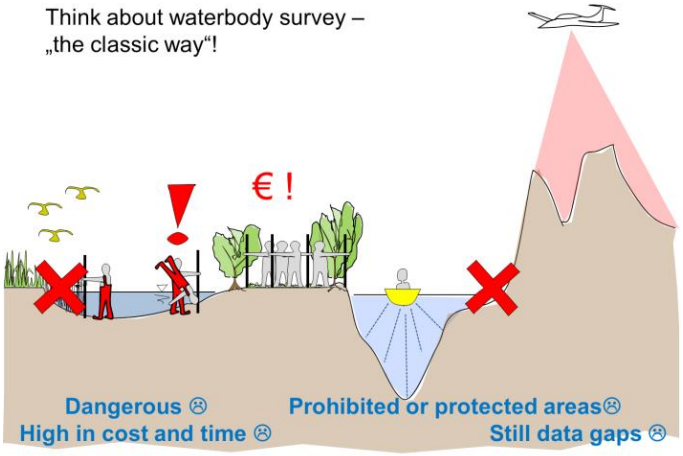

Figure 1: The classic and complex procedure of waterbody and foreland surveying.

2 HYDROMAPPING OF THE AHR TORRENT

In this study, a newly available, water-penetrating airborne laser system (green wavelength, FFG research project between the University of Innsbruck and Riegl LMS, (Fig. 2) was used to survey the alpine Ahr torrent between Sand in Taufers and Bruneck, South Tyrol, Italy, at a length of about 20 km (Fig. 3). The survey was performed in December 2012 and took 2 hours in total. The data acquisition by fixed wing aircraft was conducted from an altitude of about 600 m above ground with a pulse repetition rate of 250 kHz and a maximum laser-pulse energy still maintaining eye-safety even for the aided eye. About 33 scan strips have been acquired yielding an average total point density of 20-40 points/m². Prior to georeferencing of the hydromapping data, the 33 scan strips need to be adjusted to each other in order to derive an internally consistent data set, e.g., no vertical and horizontal offsets among strips. The uncertainty of this adjustment was about 6 cm (standard deviation). The entire point cloud is then georeferenced to UTM 32N coordinates using five terrestrially measured reference planes distributed across the project area in Fig. 3. The locations of the reference planes were selected based on the hydromapping data, and the planes were defined by the four outer corners of crosswalks. The uncertainty of the georeferencing process was about 3 cm (standard deviation). Lastly, the point cloud was classified according to Fig. 4, and the correction of the water-depth (refraction) was applied to points located below the actual water-surface level by using the software HydroVISH.

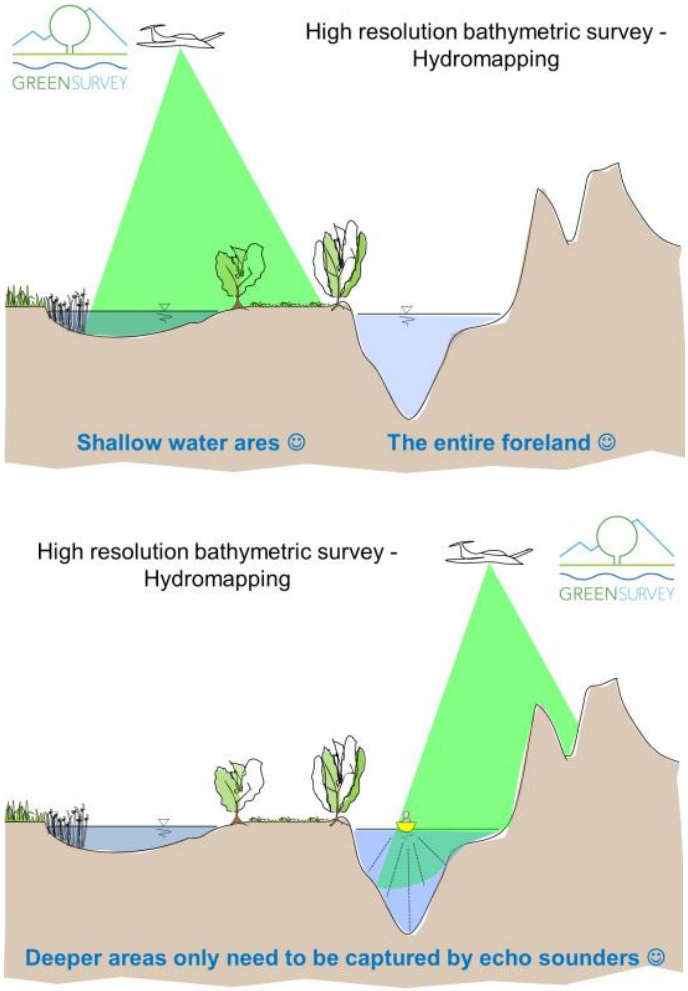

Figure 2: Shallow areas captured by hydromapping, deeper areas captured by echo sounder.

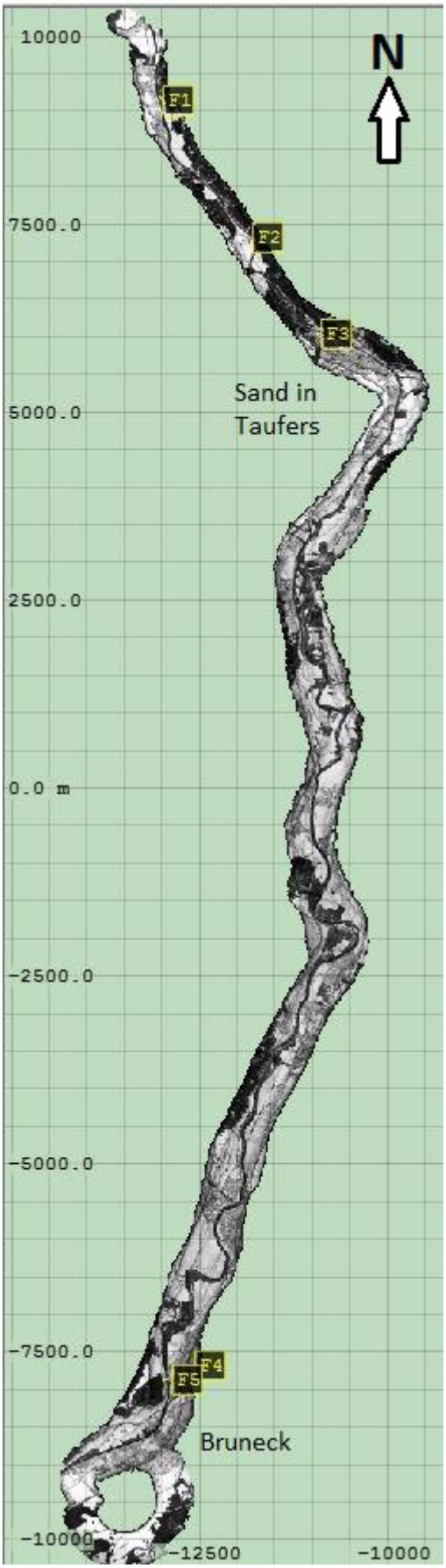

Figure 3: Project area along the Ahr torrent, South Tyrol. Yellow labels depict the reference planes for georeferencing. (RiProcess 1.5.9, RIEGL©)

3 MESH CREATION

For data evaluation, mesh construction and visualization the software framework HydroVISH, based on VISH (The Vish Visualization Shell; Benger, Ritter, & Heinzl 2007) was used. **HydroVISH** allows to combine a wide variety of different data sources, observational as well as computational ones. It is a flexible c++ programming environment where data manipulation modules can be added or extended easily. Several modules supporting manipulation, computation and visualization of point clouds are already provided.

The point cloud of the river Ahr in South-Tyrol consists of 23.1_106 points and was classified according to the following properties: ground, structure, river-bed, bank and water surface, illustrated in Fig. 4. The discharge rate (12.12.2012; South Tyrol 2012) was 12.00 m³/s. The part of the river considered for the numerical simulation is approximately 20 km long. The foreland is only partly included in the CFD simulation.

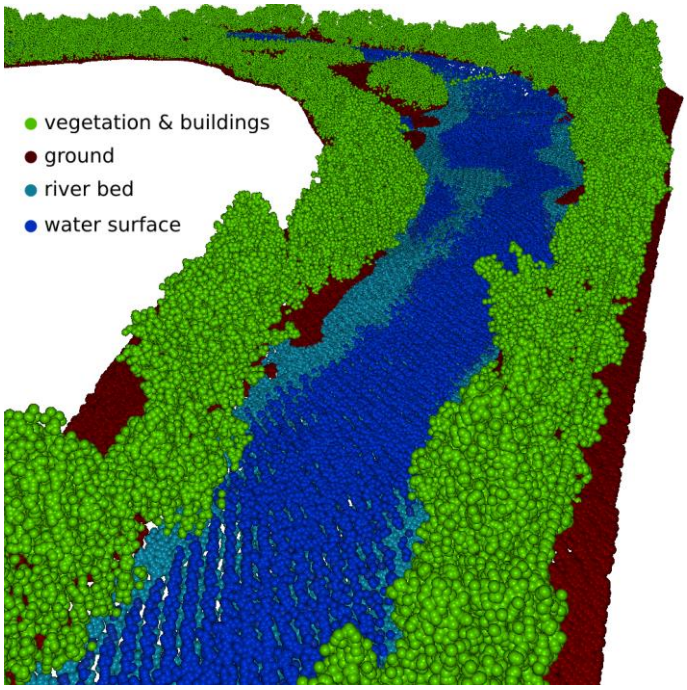

Figure 4: Detail view of the point cloud of the river Ahr. The colors represent different point classes.

The main task is now to reduce the density of the point cloud to an appropriate and easily-handled size without loosing to many features of the river bed. The first step therefore, to get a 2D-mesh, is to use only the ground-, river bed- and bank points (for convenience these points are called ”ground-points” in the next pages). Even though the LIDAR-Measurement yielded good results along the river bed, there exists still some smaller spots where no ground-points at all could be gained. This happens because of too much white water and thus, the laser

beam could not penetrate the water surface or a very dense vegetation overhanging into the river.

Empty spots in the point cloud need to be filled up which was done as follows: The first step is to map the point cloud to a uniform grid and use the flood-fill algorithm (Bradski 2008) to mark the surrounding cells around the point cloud as outside. The second step is to fill all empty cells which are not marked as outside with the mean value height of the neighbouring cells (see Fig. 6). The newly created points (cell-centered) are added to the original point cloud as is shown in Fig. 5.

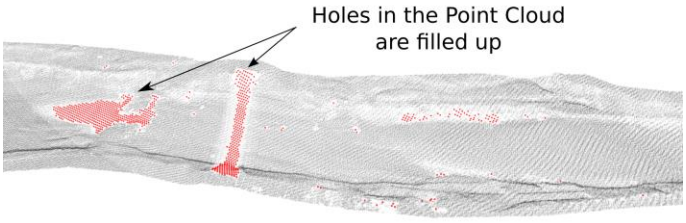

Figure 5: Red points are artificial points to close holes in the point cloud.

data	data	data	data	data	data	data
data	data	data	NW	N	NE	data
outside	data	data	W	empty cell	E	data
outside	data	data	SW	S	SE	data
outside	data	data	data	data	data	data
outside	outside	outside	data	data	data	data

Figure 6: Kernel to close holes. Mean value of the eight directions (N,NE...) are used to fill up the empty cell.

3.1 *Mesh based on breaking edges*

In order to create a mesh based on breaking-edge lines it is necessary to map the point cloud again on a uniform grid (cell size: 0.5 m, see Fig. 8, a). Afterwards, a Gaussian smoothing is applied to the uniform grid to smooth out any strong peaks. With the application of the Sobel-Operator (Soille 2003) the gradient of the image intensity (Fig. 8, b) is calculated. In order to get the breaking-edge lines a threshold value (Fig. 8, c) for the gradient of the image intensity is defined. The final step then is the usage of the marching-square algorithm (Foley, Hughes, van Dam, Feiner, McGuire, & Sklar 2013) to get the Iso-Line (breaking-edge lines) based on the intersection of the threshold value with the image intensity field (Fig. 8, d). A triangulation is done with the breaking-edge lines in Blue Kenue (3.3.4) and with the ground-points of the point cloud the height information is mapped on these triangles (Fig.7).

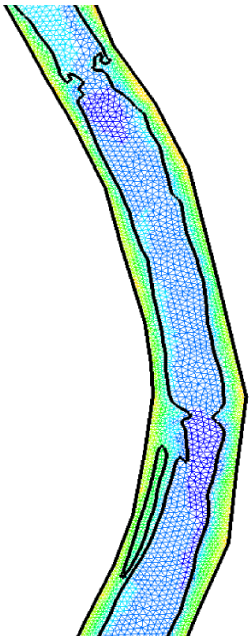

Figure 7: Mesh, based on breaking edges. Blue Kenue is used to triangulate between the breaking-edges (edge length of triangle: 1 to 3 [m]).

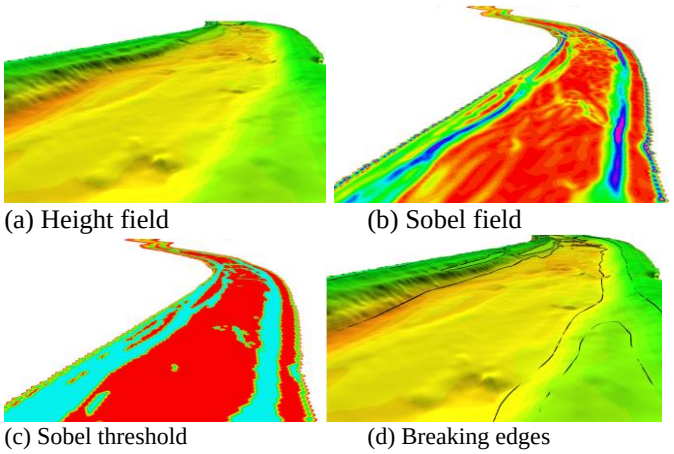

(a) Height field (b) Sobel field

(c) Sobel threshold (d) Breaking edges

Figure 8: Image based edge detection using smoothing, the Sobel-Operator, thresholding and isolines.

3.2 *Mesh based on downsampling of the point cloud*

Due to the dense populated ground-points a downsampling of the point cloud on a uniform grid has been carried out. In order to capture the majority of the features of the point cloud geometry the downsampling was done with two different cell sizes: a larger cell size (3 m edge length) for flat areas and a smaller cell size (1.5 m) for non-flat areas. To distinguish if a smaller or a larger grid should be

used a "point distribution tensor" was calculated. In (Ritter & Benger 2012) the "point distribution tensor" is defined as a set of N points $\{P_i: i = 1;\ldots;N\}$ as:

$$S(P_i) = \frac{1}{..} \sum_{k=1}^{N} \omega_{ik}(|t_{ik}, r|)\,(t_{ik} \otimes t_{ik}^{\tau}) \qquad (1)$$

whereby $\otimes$ denotes the tensor product, τ the transpose and $t_{ik} = P_i - P_k$. The term $\omega_{ik}(|t_{ik}|,r)$ is a weighting function, where r is an user specified distance or radius defining the neighborhood of a point P_i. The weighting function ω_{ik} is zero outside this radius. The distribution tensor is symmetric and positive with three eigen-values. These values are used to classify the tensor via three shape factors (Westin et al. 1997), characterizing the shape of a fitting ellipsoid of the point neighborhood. The three shape factors are:

$$\begin{aligned} c_{linear} &= (\lambda_3 - \lambda_2) / (\lambda_1 + \lambda_2 + \lambda_3) \\ c_{planar} &= 2\,(\lambda_2 - \lambda_1) / (\lambda_1 + \lambda_2 + \lambda_3) \\ c_{spherical} &= 3\,\lambda_1 / (\lambda_1 + \lambda_2 + \lambda_3). \end{aligned} \qquad (2)$$

In Eq. 2 the coefficient c_{planar} was used to distinguish between flat areas or areas where points are dispersed (see Fig. 10). Based on a threshold value a grid with different cell size (either edge length 3 m or 1.5 m) is constructed (see Fig. 9) and the mean height of the corresponding points in the cell are mapped on the grid.

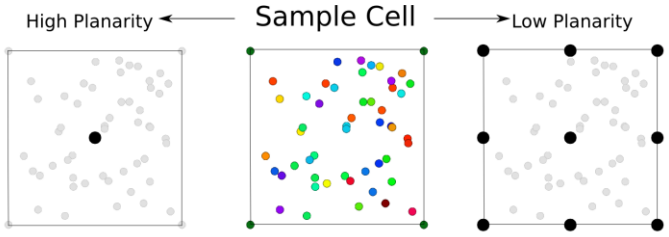

Figure 9: Downsampling of the point cloud: If the planarity of the sample is high all points are replaced by a single point with its mean height, otherwise a subgrid with cell size of 1.5 m is used.

Finally, with the qhull algorithm (Barber, Dobkin, & Huhdanpaa 1996) the downsampled points are triangulated. To avoid triangulation outside of the domain a threshold value (max. cell size is 3 m, thus threshold value of $(3^2+3^2)^{0.5}$ for the edge length is used. The resulting triangulation is shown in Fig. 11. This mesh will be exported as a SMS : 2dm file and imported in BlueKenue (3.3.4) for further processing. Note: The downsampled mesh will be used for the calibration of the CFD simulation.

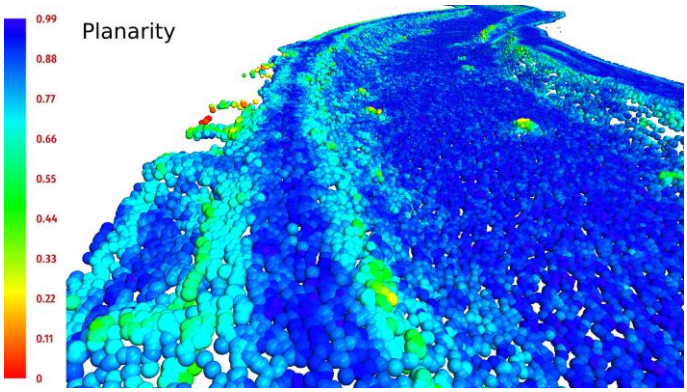

Figure 10: Planarity of the point cloud: Blue denotes good planarity (points are aligned with a plane) and red means no planarity at all.

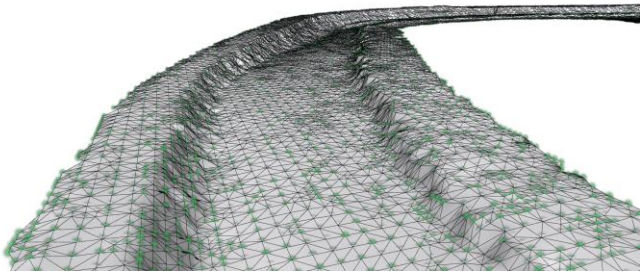

Figure 11: Triangulation of the point cloud.

3.3 *Calibration of the Telemac2D-simulation*

The CFD-Simulation was carried out with the open-source software Telemac2D (6.2). The boundary-conditions were set with BlueKenue (3.3.4) where the inlet-outlet discharge rate was Q = 12.00 m³/s and the corresponding height were derived from the LiDAR-Measurement. The mesh-dependency was checked with a 20% coarser mesh-size and for the turbulence model the k-_ and the constant eddy viscosity were tested; the comparison showed no significant differences. For the final calibration-run the constant eddy viscosity was chosen (eddy viscosity: 0.1 m²/s).

The value for the friction coefficient (Strickler-value) was automatically calculated by comparing the instantaneous water height from the CFD calculation with the target height of the hydromapping water surface. If the CFD water height was higher than the target height from the measurement, the roughness value was changed to a smoother value and vice versa. This procedure was carried out for every hour physical run-time and the corresponding value change of the roughness was not more than 5%. An upper and lower limit of the roughness with 100 and 10 $m^{1/3}/s$ was used, respectively. If the current water surface was within the range of ±2 cm of the target height no roughness changes were applied. If no target height is available for a mesh-node the mean roughness of 35 $m^{1/3}/s$ is used. After 20 hour

physical time the simulation reached a steady state condition with constant values for in- and outlet discharge, water heights and roughness values. The algorithm for the roughness correction was written in Fortran (the subroutine corstr.f, provided by Telemac2D, was altered for that purpose) and linked with the executable binary of Telemac2D.

For the target height of the LiDAR-measurement a new uniform grid was calculated. The reason for the new grid is shown in Fig. 12: The LiDAR points belonging to the water surface had been extracted within a band of 15 cm. These points are split up into cells of 3x3 m. Only the upper most points (99% quantile) are valid water surface points (Mandlburger, Pfennigbauer & Pfeifer 2013) and therefore, all water surface points are replaced by a new single point with cell centered coordinates and $z=q_{0.99}$. The newly created uniform grid is then again mapped to the original CFD-mesh to get a second CFD-mesh to compare the actual- and the target water height at each node during the numerical simulation. Almost 50 % of the target height-mesh is derived from the mapped LiDAR points Note: For very shallow waters, that is less than 15 cm, no water surface point can be measured.

The result for the automatically estimated Strickler-values are shown in Fig. 13: The range is between 50 and 25 $m^{1/3}/s$ for the detail view, whereas the mean value for the whole domain is 35 (compare also with the areal image of the river Ahr in Fig. 14). The resulting water surface based on the estimated roughness is shown in Fig. 15. The difference between LiDAR and CFD-Surface is in acceptably agreement with a mean value of 5 and a standard deviation of 11 cm (Fig. 16) which are slightly higher than the accuracy of the stripe adjustment with 6 cm. The problem is found within the scan date, not presenting the entire water surface based on the scanning technology. Shallow areas, with water heights below 15 cm, are not presenting a measured water surface. Therefore, within a further research step an algorithm was developed to reconstruct the missing water surface between the last water surface points and the main land.

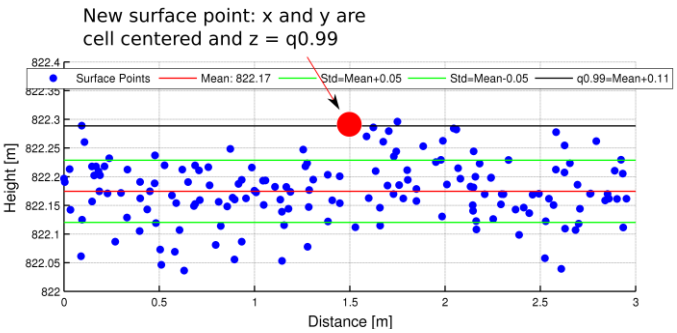

Figure 12: Water surface points within a example cell of 3x3 m: Points will be mapped on a uniform grid (cell centered). The offset from the mean value is $q_{0.99}$ = 11 cm for this example cell.

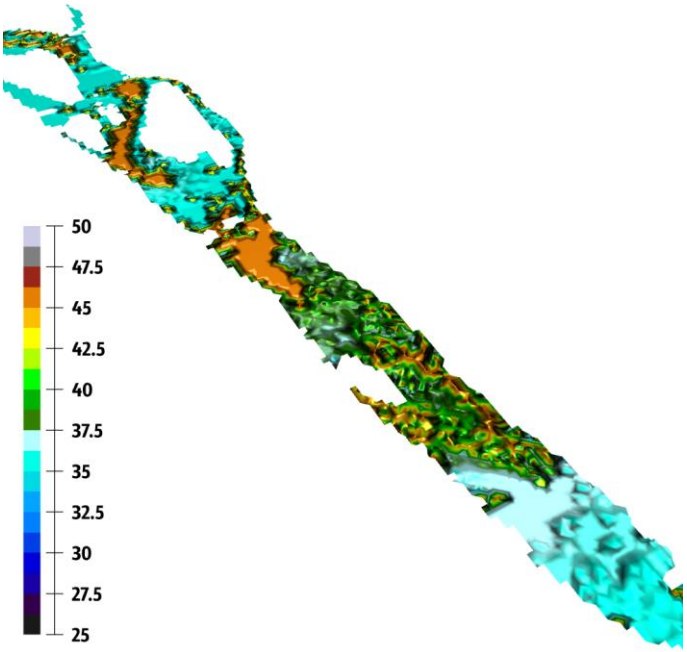

Figure 13: Estimated Strickler-value [$m^{1/3}/s$] based on the water surface comparison of LiDAR and CFD. Shown is only the wetted river bed.

Figure 14: Areal Image of the river Ahr: Strickler-value, based on the image, is approx. 30-40 $m^{1/3}/s$.

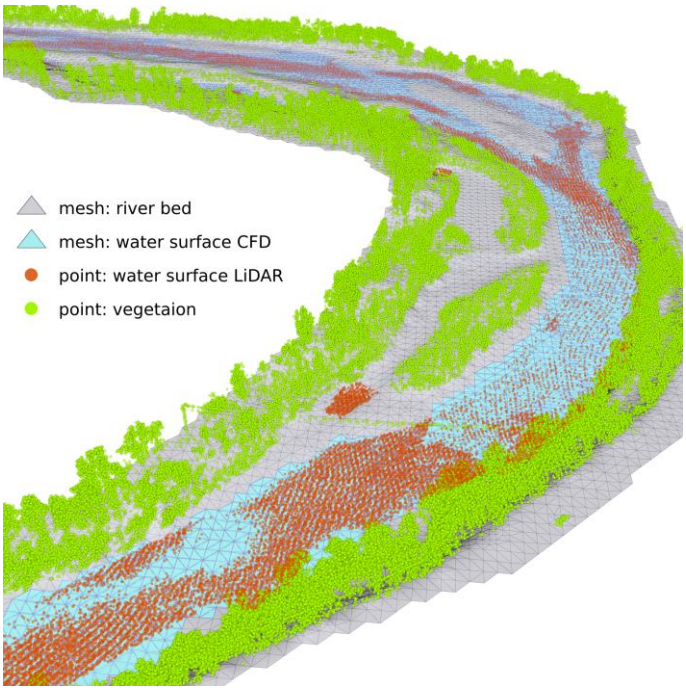

Figure 15: Detail view of the comparison of the LiDAR- and CFD-Surface.

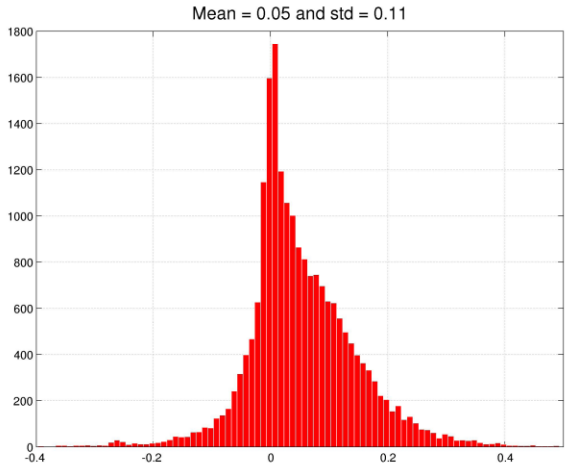

Figure 16: Differences of target height and CFD water height. Mean value is 5 and standard deviation is 11 cm.

4 CONCLUSIONS

The highly dense populated LiDAR data with an accuracy of ±6 cm (relative accuracy, derived from the strip adjustment) are very suitable for a numerical simulation. To reduce the amount of information of the point cloud a downsampling on a uniform grid with two different cell sizes has been done. In order to switch between the bigger or smaller cell size of the uniform grid a point distribution tensor was calculated; if the points are aligned to a plan (planarity is high) the bigger cell size is used, otherwise the smaller cell size is used (low planarity). The downsampled points can be easily triangulated by a qhull algorithm and exported as a 2DM (SMS) mesh for further boundary treatment in BlueKenue.

The calibration of the CFD simulation was done by using the water surface points of the airborne laser scanning. Further treatment of the water surface points are necessary due to the fact that the exact water surface needs to be calculated out of a measured water surface band of about 15 cm. Therefore, only the topmost water surface points (99% quantile) are used to create an additional target height-mesh. The calibration was finally done by comparing the target height with the heights of the resulting numerical simulation at every hour physical runtime; if the heights at each node were not equal, the roughness parameter were slightly changed to lift or reduce the water surface. Approximately 50% of the domain was covered with LiDAR heights, the rest of the domain had a constant mean roughness of 35 $m^{1/3}/s$. The results of the comparison between the target height and the height calculated by Telemac2D showed acceptable agreement, where the mean value is 5 cm and the standard deviation 11 cm (water depth is in the range of 0.15 to 2.5 m). A possible further task is to reduce the slightly higher standard deviation of 11 cm, which can be achieved by calculating the roughness value also for the remaining nodes with an unknown water height from the LiDAR measurement. These nodes mostly have a water depth lower than 15 cm, which cannot be captured by the laser device. The reconstruction of these missing water surface points and their becoming part of the comparison module within the hydraulic software is most relevant. The final solution for an automatic roughness detection by the comparison of an measured and CFD-calculated water surface is seen in this missing step.

5 REFERENCES

Barber, C. B., D. P. Dobkin, & H. T. Huhdanpaa (1996). The Quickhull algorithm for convex hulls. 2, 469–483+.

Benger, W., G. Ritter, & R. Heinzl (2007). The Concepts of VISH. In 4th High-End Visualization Workshop, Obergurgl, Tyrol, Austria, June 18-21, 2007, pp. 26–39. Berlin, Lehmanns Media-LOB.de.

Bradski, A. (2008). Learning OpenCV, [Computer Vision with OpenCV Library ; software that sees] (1. ed. ed.). O'Reilly Media. Gary Bradski and Adrian Kaehler.

Foley, J., J. Hughes, A. van Dam, S. Feiner, M. McGuire, & D. Sklar (2013). Computer Graphics: Principles and Practice. The systems programming series. Addison-Wesley.

Mandlburger, G., M. Pfennigbauer, & N. Pfeiffer (2013). Analyzing near water surface penetration in laser bathymetry – a case study at the river Pielach. In ISPRS Annals of the Photogrammetry, Remote Sensing and Spatial Information Sciences, Volume II-5/W2, pp. 175–180. poster presentation: ISPRS Workshop Laser Scanning 2013, Antalya, Turkey; 2013-11-11 – 2013-11-13.

Ritter, M. & W. Benger (2012, June). Reconstructing Power Cables From LIDAR Data Using Eigenvector Streamlines of the Point Distribution Tensor Field. In Journal of WSCG Vol20., No.3, Page 71, 20-th International Conference in Central Europe on Computer Graphics, Visualization and Computer Vision, Plzen, Czech Republic.

Soille, P. (2003). Morphological Image Analysis: Principles and Applications (2 ed.). Secaucus, NJ, USA: Springer-Verlag New York, Inc.

South Tyrol (2012). Province of Bolzano, gage height and discharge rate, www.provinz.bz.it.

Westin, C., S. Peled, H. Gudbjartsson, R. Kikinis, & F. Jolesz (1997, Apr.). Geometrical diffusion measures for mri from tensor basis analysis. In Proceedings of ISMRM, Fifth Meeting, Vancouver, Canada.